Fabrication of Functional Metallic Nanowires Using Electrodeposition Technique

Takeshi Ohgai
Nagasaki University
Japan

1. Introduction

The array of numerous metallic nanowires with straight shape has much attention due to their shape anisotropy and extremely large surface area. This unique structure can be applied to develop the novel functional nano-materials such as electronic, magnetic and optical nano-scale devices. Metallic nanowires can be fabricated by manipulating metallic atoms one by one using a scanning tunneling microscope (STM) probe, while they can be also prepared by electrochemically depositing metallic atoms into a nanoporous template with numerous cylindrical nanopores. In a fabrication technique using electrodeposition of nanowires, nanoporous templates such as anodized aluminum oxide films with high density of nanopores (about 10^8~10^{10} pores•cm^{-2}) have been used so far.

In 1975, using an anodic oxide coating film on aluminum, magnetic properties of electrodeposited Co nanowires and Co-Ni alloy nanowires were investigated (Kawai & Ueda, 1975). In 1986, as an application to perpendicular magnetic recording medium, alumite films containing Fe nanowires were fabricated (Tsuya et al., 1986). In 1988, magnetization curling process in perpendicular direction was studied using Fe nanowire arrays in alumite media (Huysmans et al., 1988). In 1990, influence of the packing density on the magnetic behaviour was investigated using alumite media containing magnetic nanowires (Zhang et al., 1990).

On the other hand, in 1991, using the polymer membrane template with numerous nanopores, polymeric and metal microtubules were synthesized (Martin, 1991). In 1993, arrays of Ni and Co nanowires were electrodeposited in polymer templates with the nanometer-sized pores prepared by nuclear track etching technique (Whitney et al., 1993). They found that the preferred magnetization direction is perpendicular to the film plane and enhanced coercivities as high as 680 Oe. Remnant magnetization of the nanowires up to 90% had been reported. In 1994, a membrane-based synthetic approach to obtain nano-materials was introduced to materials science field (Martin, 1994). He suggested that the template synthesis method is useful to prepare polymers, metals, semiconductors, and other materials on a nano-scopic scale.

In 1994, giant magnetoresistance (GMR) properties were found in Co/Cu multilayered nanowires electrodeposited in nanoporous polymer template (Piraux et al., 1994). In the report, magnetoresistance measurements with the current perpendicular to the layers were performed on the array of parallel nanowires. They observed that the 15% of GMR at room temperature on Co/Cu multilayered nanowires. In the almost same time, GMR of

nanowires with Co/ Cu and Ni-Fe/ Cu multilayers was demonstrated (Blondel et al., 1994). They made the multilayered nanowires with 6 µm long, 80 nm in diameter and each layer thickness of 5–10 nm in nanoporous polymer template. At ambient temperature, GMR of 14% for Co/ Cu and of 10% for Ni-Fe/ Cu was demonstrated in the current perpendicular to the layers.

On the contrary, in 2000, current perpendicular to plane giant magnetoresistance (CPP-GMR) was found using the multilayered nanowires electrodeposited in a commercially available anodic aluminum oxide membrane filter (Evans et al., 2000). In the report, Co–Ni–Cu/ Cu multilayered nanowires were synthesized and extremely large values (55% at room temperature and 115% at 77 K) of CPP-GMR were demonstrated. In 2003, Co/ Cu multilayered nanowires with spin-valve effect and GMR response were synthesized in self-organized anodized aluminum oxide nanopores grown at the surface of bulk aluminum (Ohgai et al., 2003). In the report, the aluminum oxide template with pore-length as short as 2000 nm was used and the pore bottom oxide layer was removed by a chemical etching technique. 20% of GMR was demonstrated in Co/ Cu multilayered nanowires at room temperature, while the typical resistance switching of spin-valves was observed in Co/ Cu/ Co tri-layered nanowires.

Compound semiconductor nanowires were also fabricated as well as ferromagnetic metal nanowires using an electrodeposition technique. Bi_2Te_3 nanowires (Wang et al., 2004), CdTe nanowires (Ohgai et al., 2005), InSb nanowires (Zhang et al., 2005) and ZnSe nanowires (Katkar & Tait, 2007) have been synthesized so far. They reported that these semiconductor nanowires can be applied to light emission diodes, photovoltaic devices, solar cells and thermovoltaic devices.

If the template synthesis technique on the basis of fabricating nanopores and electrodepositing nanowires as mentioned above is applied to produce micro- and nano-scale devices in ultra large scale integration (ULSI), position of each nanopore, inter-pore distance, pore diameter and pore shape should be controlled precisely. To fabricate novel electronic devices in ULSI, lithographic galvanoforming (LIGA) process using laser, UV, X-ray, electrons and ions can be used.

In this chapter, fabrication process such as electrodeposition behavior, morphology, crystal structure and magnetic properties (magnetization and magnetoresistance) of metallic nanowires such as Ni, Co, Fe (in section 2), Ni-Fe alloy (in section 3) and Co/ Cu multilayer (in section 4) were discussed for the application to novel functional micro- and nano-scale devices.

2. Ni, Co and Fe nanowires

2.1 Electrodeposition process of Ni, Co and Fe nanowires

Ion track-etched polycarbonate membrane filters with pore-diameter of 40, 80, 160 and 300 nm, pore-length of 6000 nm and pore-density of 10^8 pore•cm^{-2} were used as a template for growing metallic nanowires as shown in Fig.1. On a surface of the membrane filter, a gold layer was sputter-deposited to cover the pores and make a cathode. Aqueous solution containing metal sulfate was used as electrolyte.

To determine the optimum deposition potential for growing nanowires, cathodic polarizarion behavior was investigated in a wide range of cathode potential. Figure 2 shows cathodic polarization curves obtained from the solutions containing each iron-group metal ions (Ni^{2+}, Co^{2+} or Fe^{2+}).
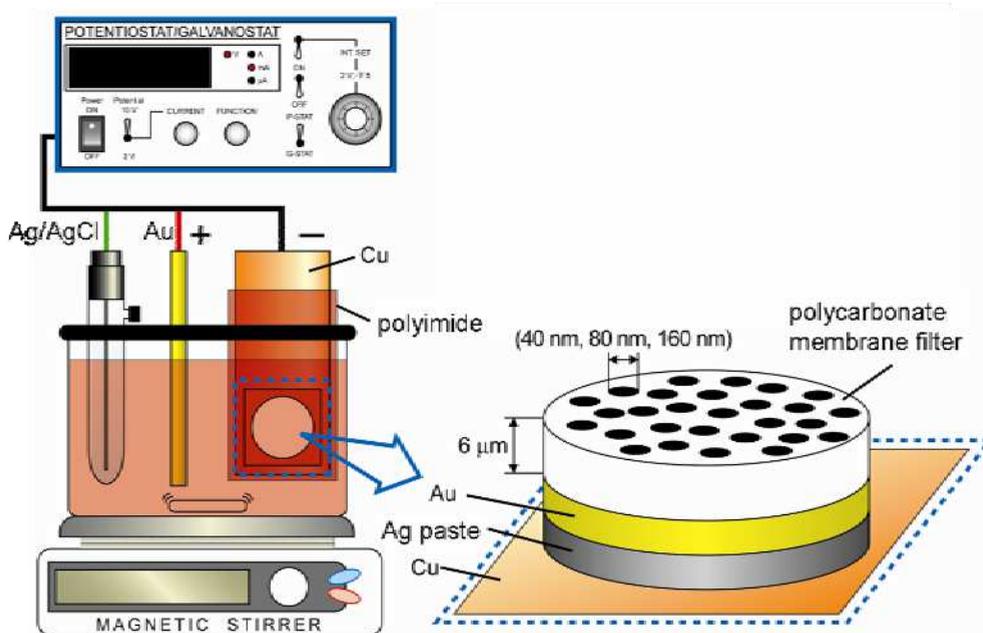
Fig. 1. Experimental apparatus for electrodepositing metallic nanowires in polycarbonate membrane filter with numerous cylindrical nanochannels.

The cathodic current begins to occur at ca. 0 V vs.Ag/ AgCl, which is more-noble than the equilibrium potential of iron-group metals. It is well known that the standard electrode potentials for Ni, Co and Fe are -0.46, -0.48 and -0.64 V vs.Ag/ AgCl. Therefore, this cathodic current is presumed to be reduction current of H^+ ions. With increasing the cathodic current, at around 10^{-3} A, the potential polarizes to be around –0.8 V due to the diffusion limit of H^+ ions.

At around –0.8 V, the cathodic current increases again. It is also well known that the electrodeposition of iron-group metals proceeds accompanying some over potential. Therefore, this increase in cathodic current is mainly caused by an increase in deposition current of iron-group metal ions. At the potential region less than –1.2 V, with increasing cathodic current, the potential polarizes significantly to be less-noble region due to the diffusion limit of iron-group metal ions.

Consequently, the optimum cathode potential region for growing iron-group metal nanowires is determined to be from –0.9 to –1.2 V according to the cathodic polarization curves as shown in Fig.2.

To investigate the growing process of nanowires, time dependence of cathodic current was monitored during the electrodeposition. Ni, Co and Fe nanowires were potentio-statically electrodeposited at room temperature. Figure 3 shows the effect of cathode potential on the time-dependence of cathodic current in the solution containing Ni^{2+} ions. During the electrodepostion of Ni, cathode potentials were fixed to –0.9, –1.0, –1.1 and –1.2 V. If the potential was kept to –1.0 V, the cathodic current reached up to ca. 1 mA at the beginning of electrolysis within several tens minutes. Then, the current rapidly decresed to be ca. 0.4 mA
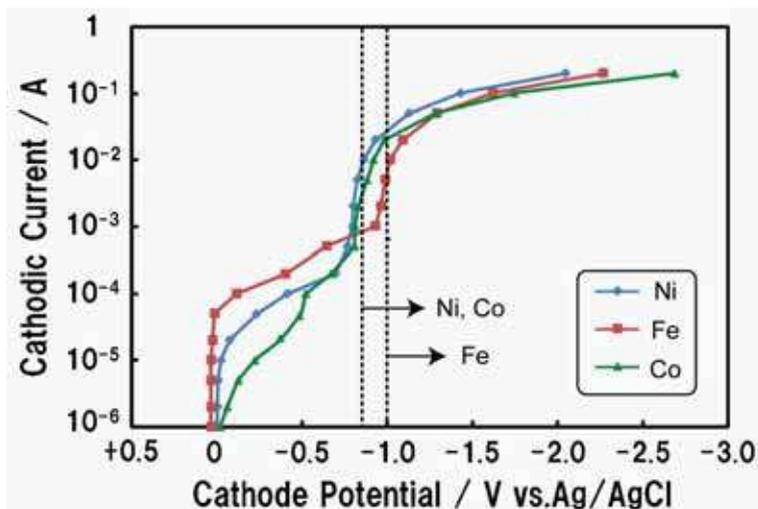
Fig. 2. Cathodic polarization curves for electrodeposition of Ni, Co and Fe on Cu sheet from aqueous solutions containing Ni^{2+} or Co^{2+} or Fe^{2+} ions.

and kept the magnitude until around 1000 sec. During this process, electrodeposition of Ni proceeds in the nanopores.

At the initial stages of the electrodepostion, large cathodic current was observed in every cathode potential. The concentration of metal ions in the nanopores will decrease with increasing electrodeposition time due to the cathodic reduction, while the metal ions will be provided from the bulk solution to the nanopore, where the metal ions are consumed by the electrodeposition.

Finally, as shown in Fig.3, the cathodic current rapidly increases at the deposition time more than 1000 sec. At this stage, electrodeposited nanowires reach the surface of the membranes and large hemispheric Ni deposits are formed. Growth rate of Ni nanowires can be estimated as ca. 6 nm•sec^{-1} at the cathode potential of –1.0 V. Time-dependence of cathodic current for Co and Fe deposition also showed similar behavior as well as Ni deposition. Growth rate of the nanowires increases up to around 30 nm•sec^{-1} with increasing cathode potential up to -1.2 V.

2.2 Crystal structure of Ni, Co and Fe nanowires

After the growing nanowires, polycarbonate membrane filters were dissolved in organic solvent (dichloromethane and chloroform) and the remains consisted of nanowires and a gold layer was served as a sample for scanning electron microscope (SEM) observation. On the other hand, using ion-milling technique, as-deposited nanowires in a membrane filter were thinned and a cross-sectional area of the nanowires was observed using transmission electron microscope (TEM).

Figure 4 shows SEM images of Co nanowires separated from the polycarbonate templates. Diameter (40, 80, 160 and 300 nm) and length (6000 nm) of the nanowires corresponds well to that of nanopores and the cylindrical shape was precisely transferred from the nanopores to the nanowires. Aspect ratio of the nanowires reaches up to around 150.
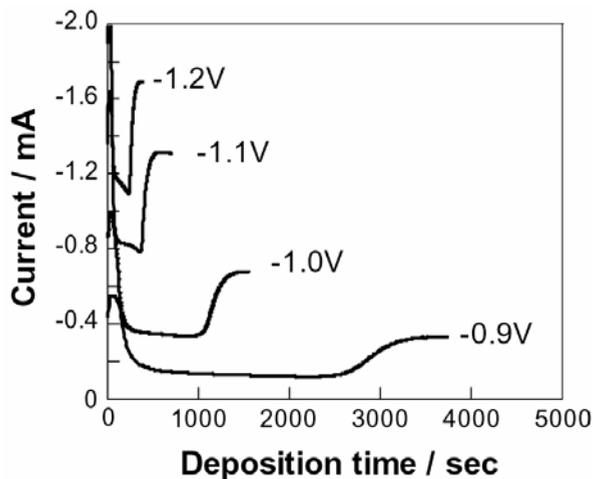
Fig. 3. Effect of cathode potential on the time-dependence of cathodic current during electrodeposition of Ni nanowires.
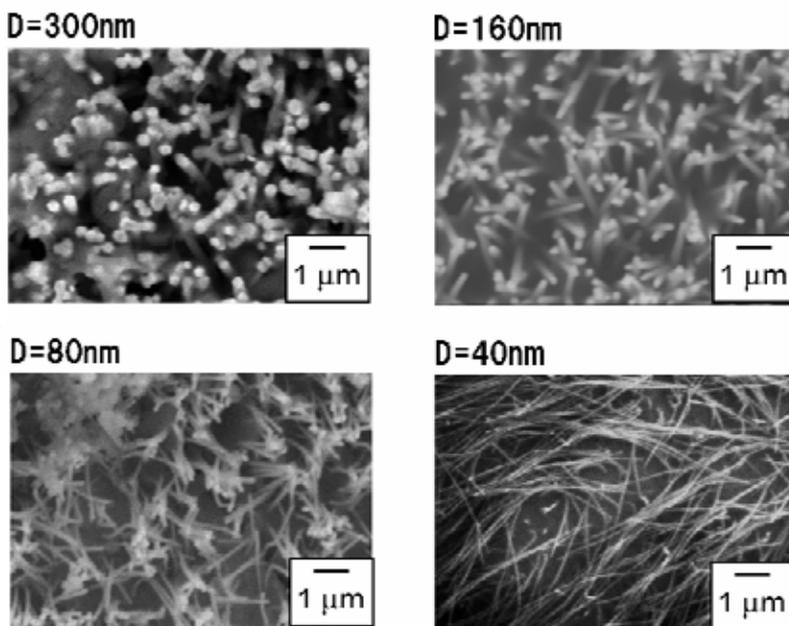

Fig. 4. SEM images of electrodeposited Co nanowires separated from polycarbonate membrane filters.

TEM bright images and diffraction patterns of electrodeposited Ni, Co and Fe nanowires were also investigated as shown in Fig.5. According to TEM bright images, cross-sectional area of the nanowire was almost to be round shape, while the diffraction patterns are composed of spots, which means a nanowire consists of a single crystal domain.
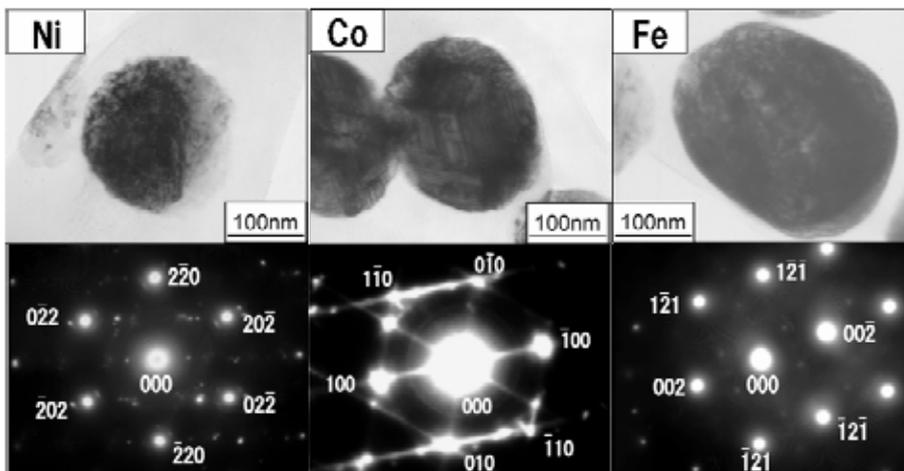
Fig. 5. Cross-sectional TEM images of Ni, Co and Fe nanowires electrodeposited in polycarbonate membrane filter.

2.3 Magnetic properties of Ni, Co and Fe nanowires

Magnetic hysteresis loops of electrodeposited nanowires were obtained using vibrating sample magnetometer (VSM) with increasing the magnetic field up to 10 kOe. Figure 6 shows the magnetic hysteresis loops of Ni, Co and Fe nanowires electrodeposited into polycarbonate templates with pore-diameter of 80, 160 and 300 nm. Magnetic field was applied to perpendicular directions to the film plan, which corresponds to the parallel direction to the long axis of nanowires. Coercive force of the nanowires was increased in decreasing the pore-diameter. Figure 7 shows the magnetic hysteresis loops of Ni, Co and Fe nanowires electrodeposited into polycarbonate templates with pore-diameter of 40 nm. As shown in these figures, magnetization switching was observed at around 1 kOe and residual magnetization was almost equal to the saturated magnetization. The coercive force of Co nanowires reaches up to 1084 Oe and the magnetic hysteresis loop shows typical perpendicular magnetization behavior. This is resulting from the uni-axial magnetic anisotropy and single magnetic domain structure of the nanowires with large aspect ratio.

3. Ni-Fe alloy nanowires

3.1 Electrodeposition process of Ni-Fe alloy nanowires

Ion track-etched polycarbonate membrane filters with pore-diameter of 80, 160, 300 and 800 nm, pore-length of 6000 nm and pore-density of 10^8 pore•cm^{-2} were used as a template for growing metallic nanowires while copper foils were used as a cathode for electrodepositing metallic films. On a surface of the membrane filter, a gold layer was sputter-deposited to cover the pores and make a cathode. Aqueous solution containing metal sulfate was used as electrolyte. The solution compositions are shown in Table 1.

To determine the optimum deposition potential for growing nanowires, cathodic polarizarion behavior was investigated in a wide range of cathode potential. Ni and Ni-Fe alloy nanowires were potentio-statically electrodeposited at 313 K. Figure 8 shows cathodic

polarization curves for the electrodeposition of Ni and Ni-Fe alloy. For the Ni-Fe alloy deposition, the solutions containing 1.5 % of Fe^{2+} ions concentration ratio ($R^{Fe/bath}$=1.5%) was used as shown in Table 1.
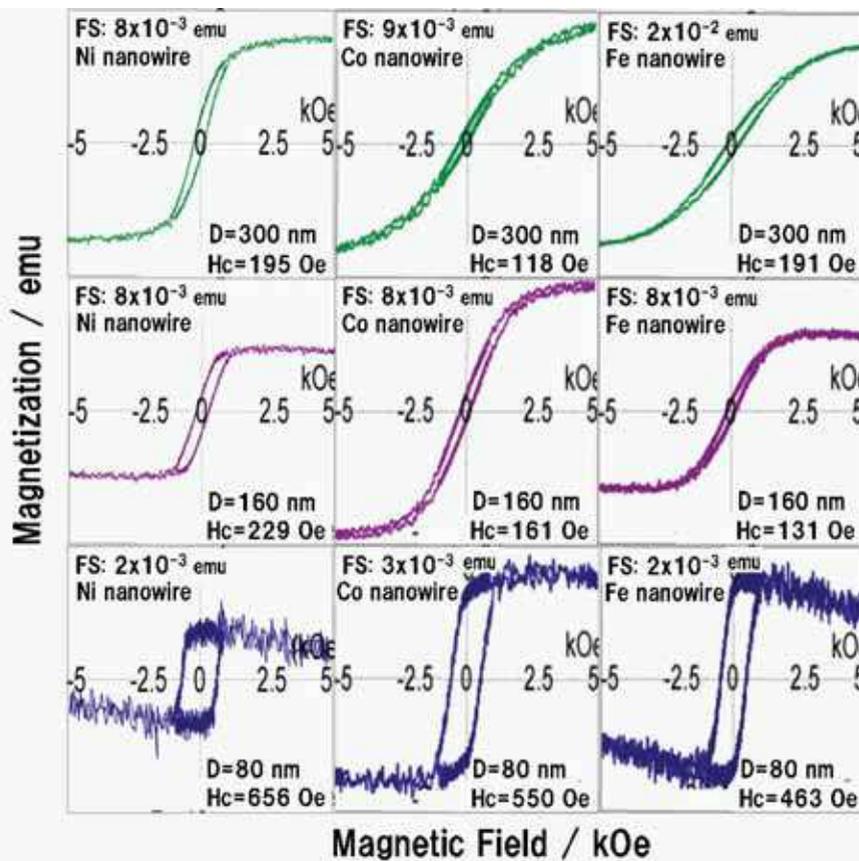

Fig. 6. Magnetic hysteresis loops of Ni, Co and Fe nanowires electrodeposited into polycarbonate templates with channel-diameter of 80, 160 and 300 nm.
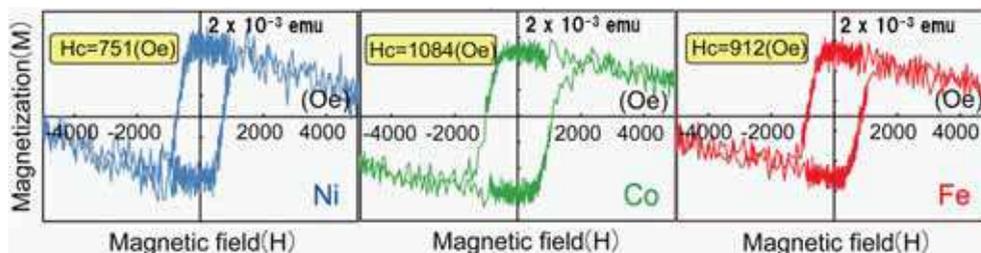

Fig. 7. Magnetic hysteresis loops of Ni, Co and Fe nanowires electrodeposited into polycarbonate templates with channel-diameter of 40 nm.

	NiSO$_4$·7H$_2$O (mol/L)	FeSO$_4$·7H$_2$O (mol/L)	H$_3$BO$_3$ (mol/L)	[Fe^{2+}] / ([Fe^{2+}] + [Ni^{2+}]) (%)
①	0.4950	0.0050	0.75	1.0
②	0.4925	0.0075	0.75	1.5
③	0.4900	0.0100	0.75	2.0
④	0.4850	0.0150	0.75	3.0
⑤	0.4350	0.0650	0.75	13.0

Table 1. Electrolytic solution composition for electrodeposition of Ni-Fe alloys.

The cathodic current begins to occur at ca. 0 V vs.Ag/ AgCl, which is more-noble than the equilibrium potential of Ni and Fe. Therefore, this cathodic current is presumed to be reduction current of H$^+$ ions. With increasing the cathodic current, at around 10^{-3} A, the potential polarizes to be around –0.7 V due to the diffusion limit of H$^+$ ions. At around –0.7 V, the cathodic current for Ni deposition increases again, while the cathodic current for Ni-Fe alloy deposition increases at around –0.8 V. This increase in cathodic current is mainly caused by an increase in deposition current of Ni and Ni-Fe. At the potential region less than –1.2 V, with increasing cathodic current, the potential polarizes significantly to be less-noble region due to the diffusion limit of Ni^{2+} and Fe^{2+} ions.

Consequently, the optimum cathode potential for electrodeposition of Ni and Ni-Fe alloys is determined to be –1.0 V.
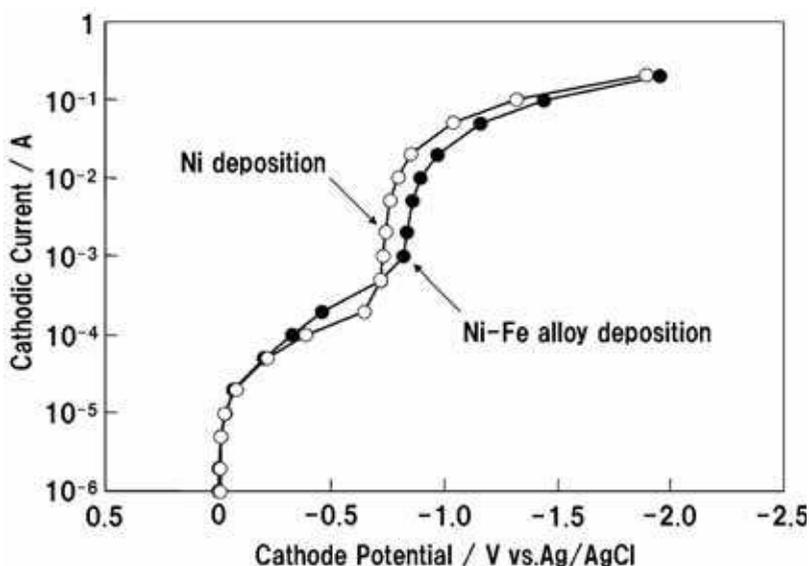

Fig. 8. Cathodic polarization curves for the electrodeposition of Ni and Ni-Fe alloy on Cu sheet from aqueous solutions containing Ni^{2+} and Fe^{2+} ions.

To investigate the relationship between Fe^{2+} concentration ratio ($R^{Fe/bath}$=[Fe^{2+}]/ ([Fe^{2+}]+[Ni^{2+}])) in baths and Fe content ($R^{Fe/depo}$ =[Fe]/ ([Fe]+[Ni])) in Ni-Fe

alloy deposits, the composition of electrodeposits were determined using EDX analysis. Figure 9 shows the relationship between Fe^{2+} concentration ratio ($R^{Fe/bath}$) in baths and Fe content ($R^{Fe/depo}$) in Ni-Fe alloy deposits. With increase in $R^{Fe/bath}$, $R^{Fe/depo}$ also increases. In the figure, composition reference line (C.R.L) means $R^{Fe/depo}$ corresponds to $R^{Fe/bath}$. In this study, less-noble Fe preferentially electrodeposited rather than Ni. For example, Ni-22at.%Fe alloy deposit ($R^{Fe/depo}$=22%) was obtained from the solution containing 1.5 % of Fe^{2+} ions ($R^{Fe/bath}$=1.5%). Fe ratio in deposit was condensed ca. 10 times higher than Fe^{2+} ratio in bath. This result can be explained by the anomalous codeposition mechanism due to the formation and adhesion of $Fe(OH)_2$ on cathode. In this mechanism, $Fe(OH)_2$ on cathode would suppress and inhibit the electrodeposition of Ni.
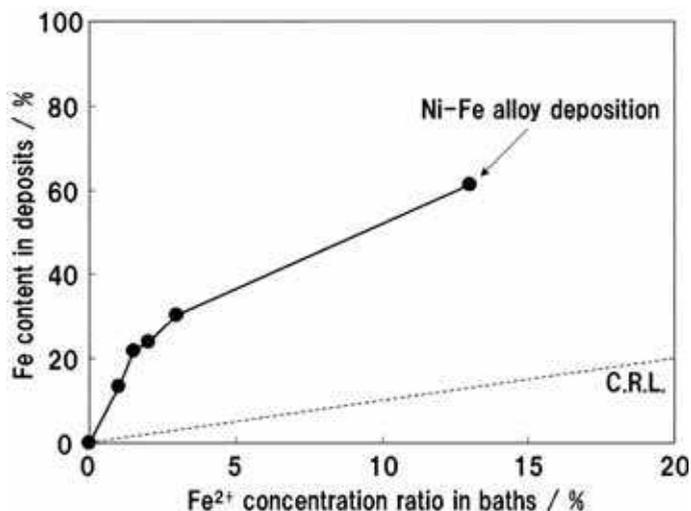

Fig. 9. Relationship between Fe^{2+} concentration ratio ($[Fe^{2+}]/([Fe^{2+}]+[Ni^{2+}])$) in baths and Fe content in Ni-Fe alloy deposits.
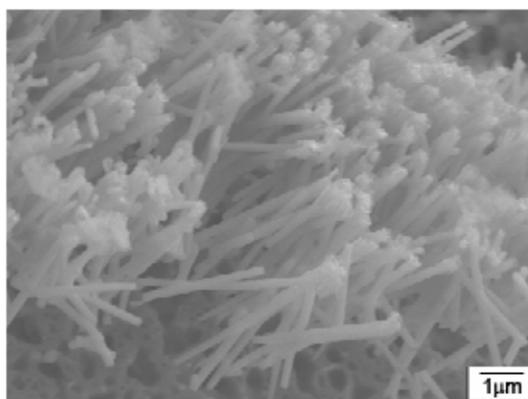

Fig. 10. SEM image of electrodeposited Ni-22at.%Fe alloy nanowires separated from polycarbonate membrane filter.

3.2 Crystal structure of Ni-Fe alloy nanowires

After the growing nanowires, polycarbonate membrane filters were dissolved in organic solvent (dichloromethane and chloroform) and the remains consisted of nanowires and a gold layer was served as a sample for SEM observation. Figure 10 shows SEM image of Ni-22at.%Fe alloy nanowires separated from polycarbonate template. Diameter and length of the nanowires corresponds well to that of nanochannels and the cylindrical shape was precisely transferred from the nanochannels to the nanowires as well as the case of pure Ni and pure Fe nanowires as shown in Fig.4.

3.3 Magnetic properties of Ni-Fe alloy nanowires

Magnetic hysteresis loops of electrodeposited films and nanowires were obtained using VSM with increasing the magnetic field up to 10 kOe. Figure 11 shows the magnetic hysteresis loops of Ni film and Ni-22at.%Fe alloy film electrodeposited on a copper foil. Magnetic field was applied to in-plan direction (red line) and perpendicular direction (blue line) to the film plan. As shown in these figures, in perpendicular direction, the films were hardly magnetized. On the other hand, in-plan direction, the films were easily magnetized and the magnetization reached to saturation at less than 1 kOe. Coercive force of Ni-22at.Fe alloy film was only ca. 1 Oe, which is quite smaller than that of Ni film (ca. 110 Oe). This is resulting from decreasing the magnetic anisotropy constant and magnetostriction constant of Ni with increase in Fe content in Ni-Fe alloy.
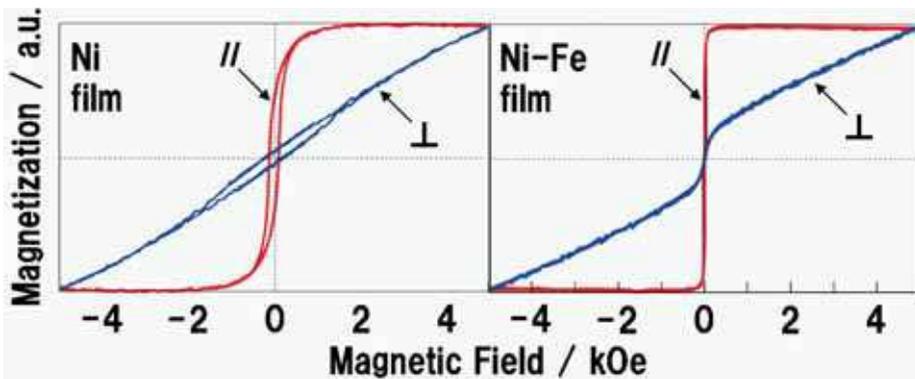

Fig. 11. Magnetic hysteresis loops of Ni film and Ni-22at.%Fe alloy film electrodeposited from aqueous solutions. Magnetic field was applied to in-plan direction (red line) and perpendicular direction (blue line) to the film plan.

Figure 12 shows the relationship between Fe content in Ni-Fe alloy deposits ($R^{Fe/depo}$) and the coercive force obtained from magnetic hysteresis loops with the applied magnetic field of in-plan direction. With increase in Fe content in deposits, the coercive force decreased down to ca. several Oe level. It is well known that coercive force, H_c is expressed by the following equation if the rotation process is dominant in magnetization.

$$H_c = 2K/ M_s \qquad (1)$$

Here, K and M_s mean magnetic anisotropy constant and saturated magnetization. Magnetic anisotropy constants of Ni and Fe are followings. K_{Ni} = -4.5 kJ/ m^3 (-562.5 kGOe) and K_{Fe} =

+48 kJ m^3 (+6000 kGOe). Saturated magnetization of Ni and Fe are followings. M_{Ni} = 0.61 T (6100 G) and M_{Fe} = 2.16 T (21600 G). Therefore, the theoretical coercive force of Ni, H_{Ni} is estimated to be around 184 Oe, which is larger than the value (ca. 110 Oe) obtained in this study. If the magnetic anisotropy constant and saturated magnetization of Ni-Fe alloy can be expressed by the following equation,

$$K_{Ni-Fe} = K_{Ni} \times (1 - R^{Fe/depo}) + K_{Fe} \times R^{Fe/depo} \tag{2}$$

$$M_{Ni-Fe} = M_{Ni} \times (1 - R^{Fe/depo}) + M_{Fe} \times R^{Fe/depo} \tag{3}$$

The theoretical coercive force of Ni-Fe alloy, H_{Ni-Fe} will be expressed by the following equation,

$$H_{Ni-Fe} = 2K_{Ni-Fe} / M_{Ni-Fe} \tag{4}$$

In this theory, Ni-9at.%Fe alloy will show minimum coercive force, which is almost zero. On the other hand, if the domain wall process is dominant in magnetization, H_c is expressed by the following equation.

$$H_c \propto \lambda\sigma / M_s \tag{5}$$

Magnetostriction constant of Ni and Fe are followings. λ_{Ni} = -2.0 $\times$ 10^{-5} and λ_{Fe} = +2.0 $\times$ 10^{-5}. In this theory, Ni-50at.%Fe alloy will show minimum coercive force, which is almost zero. In this study, as shown in Figure 4, the Ni-Fe alloy films with low coercive force were obtained over the wide range of Fe content from 20 % to 60 %.
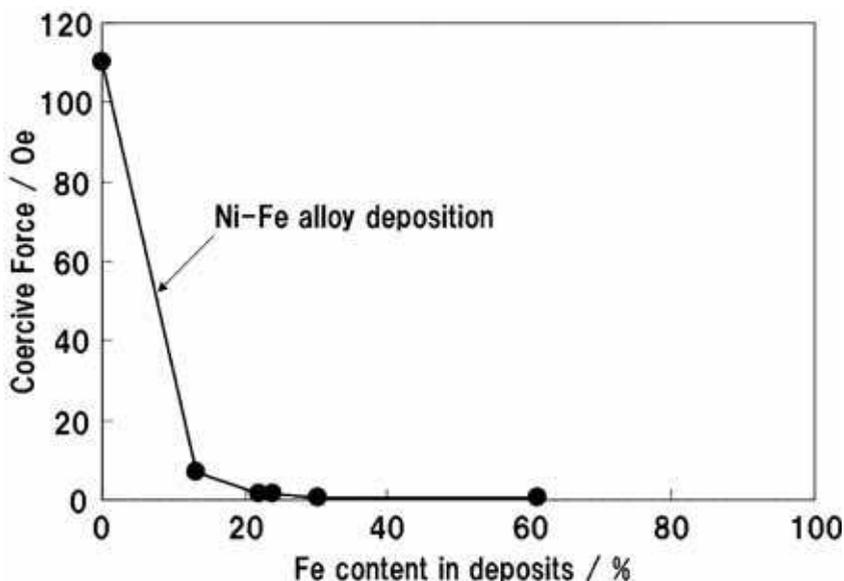

Fig. 12. Relationship between Fe content in Ni-Fe alloy deposits and the coercive force obtained from magnetic hysteresis loops of the alloy.

Figure 13 shows the magnetic hysteresis loops of Ni and Ni-22at.%Fe alloy nanowires electrodeposited into polycarbonate templates with channel-diameter of 160 nm. Magnetic field was applied to in-plan direction (red line) and perpendicular direction (blue line) to the membrane film plan. The perpendicular direction to the membrane film plan corresponds to the parallel direction to the long axis of nanowires.

As shown in these figures, in-plan direction, the nanowires were hardly magnetized. On the other hand, in perpendicular direction, the nanowires were easily magnetized and the magnetization reached to saturation at less than 2 kOe. Coercive force of Ni-22at.Fe alloy nanowires was ca. 100 Oe, which is almost half value of Ni nanowires (ca. 200 Oe) and the magnetic hysteresis loops show unique soft magnetic behavior. This is resulting from decreasing the uni-axial magnetic anisotropy due to the alloying effect of Fe. According to the equation (2), K_{Ni-Fe} will decrease with increasing the content of Fe. On the other hand, due to the equation (3), M_{Ni-Fe} will increase with increasing the content of Fe. Consequently, H_{Ni-Fe} will decrease with increasing the content of Fe according to the equation (4).

Figure 14 shows the magnetic hysteresis loops of Ni nanowires and Ni-22at.%Fe alloy nanowires electrodeposited into polycarbonate templates with channel-diameter of 80, 160, 300 and 800 nm. Magnetic field was applied to perpendicular directions to the film plan, which corresponds to the parallel direction to the long axis of nanowires.

According to the figures, coercive force of Ni-22at.%Fe alloy nanowires was decreased with increasing the channel-diameter as well as the case of Ni nanowires. The coercive force of Ni-22at.%Fe alloy nanowires with channel-diameter of 800 nm reached down to 58 Oe. The magnetic hysteresis loop of the alloy nanowires shows unique linear dependence over the wide range of magnetic field.
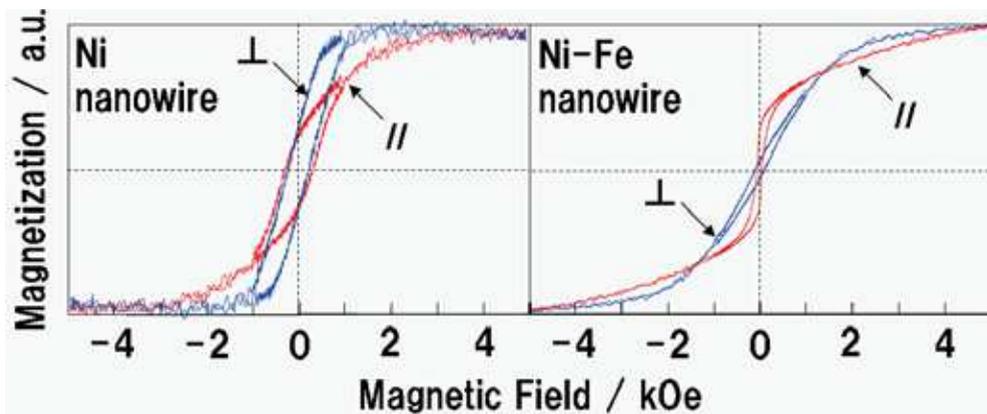

Fig. 13. Magnetic hysteresis loops of Ni nanowires and Ni-22at.%Fe alloy nanowires electrodeposited into polycarbonate templates with channel-diameter of 160 nm. Magnetic field was applied to in-plan direction (red line) and perpendicular direction (blue line) to the membrane film plan. The perpendicular direction to the membrane film plan corresponds to the parallel direction to the long axis of nanowires.
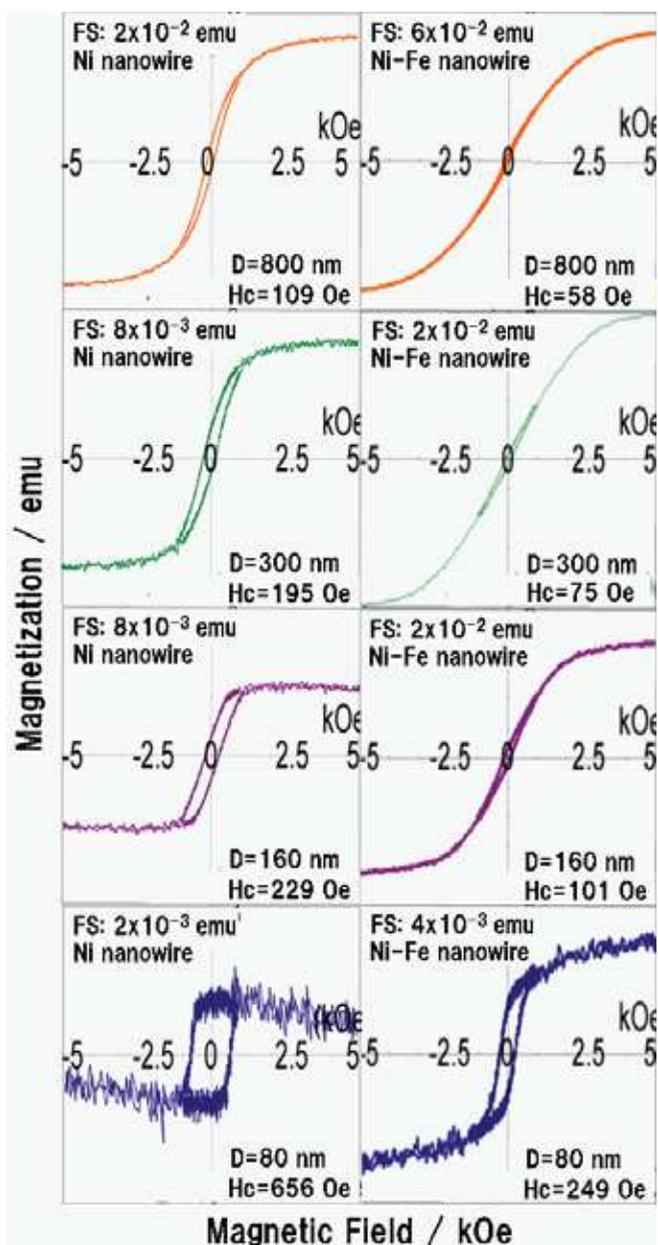
Fig. 14. Magnetic hysteresis loops of Ni nanowires and Ni-22at.%Fe alloy nanowires electrodeposited into polycarbonate templates with channel-diameter of 80, 160, 300 and 800 nm. Magnetic field was applied to perpendicular directions to the film plan, which corresponds to the parallel direction to the long axis of nanowires.

4. Co/Cu multilayered nanowires

4.1 Electrodeposition process of Co/Cu multilayered nanowires

Figure 15 illustrates the fabrication process of Co/ Cu multilayered nanowires electrodeposited in nanochannels obtained by the heavy-ion track etching technique applied in this study: (a) recording of heavy ion tracks, (b) etching of tracks, (c) formation of electrodes, (d) electrodeposition of Co/ Cu nanowires.

First, by irradiating the sample with an ion beam from a linear accelerator, straight ion tracks with a density of 10^8 tracks cm^{-2} were created perpendicular to the film surface as shown in Fig.15-(a). The tracks were selectively etched in a 6 M aqueous solution of NaOH to produce cylindrical nanochannels as depicted in Fig.15-(b). The etching process following the irradiation was optimized to produce a uniform cross section all along the channel with very small roughness.

A copper layer of thickness 1 μm, which acts as cathode for the nanowire growth, was electrodeposited on a gold layer of thickness 100 nm sputtered on the membrane as shown in Fig.15-(c). An aqueous electrolytic solution was synthesized from CoSO$_4$•7H$_2$O 120 g L^{-1}, CuSO$_4$•5H$_2$O 1.6 g L^{-1} and H$_3$BO$_3$ 45 g L^{-1} for electrodeposition of Co-Cu alloy nanowires and Co/ Cu multilayered nanowires as shown in Fig.15-(d).

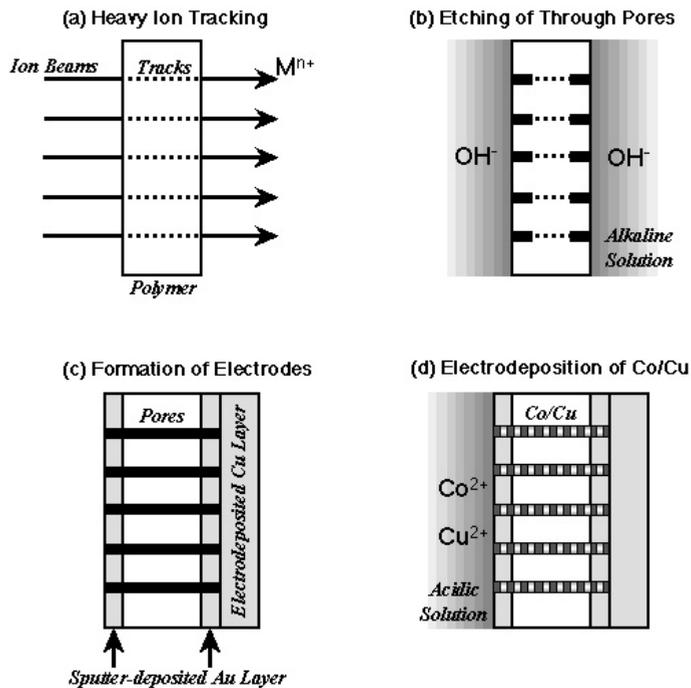Fig. 15. Schematic of fabrication process of Co/ Cu multilayered nanowires electrodeposited in nanochannels obtained by heavy-ion-track etching: (a) preparing latent tracks using heavy-ion beams, (b) etching of latent tracks leading to channels, (c) sputtering a gold layer on both sides of the surface and electrodeposition of Cu layer on the sputtered gold layer, (d) electrodeposition of Co/ Cu nanowires in the channels.

A cathodic polarization curve was measured over a wide range of cathode potential to determine the optimum potential for Cu and Co deposition.

Figure 16 shows a cathodic polarization curve of polycarbonate template with channel length 30 μm and diameter 200 nm. The equilibrium potentials of Cu and Co are estimated to be around +0.05 V and –0.48 V (vs.Ag/ AgCl) on the basis of the Nernst equation as follows.

$$E^{eq} = E^0 + RT (nF)^{-1} \ln C_M \tag{6}$$

Here, E^0 is the standard electrode potential, and C_M denotes the concentration of metal ions (Cu^{2+} or Co^{2+}).

The cathodic current occurs at the potential region close to the equilibrium potential of Cu as shown in Fig.16. It is well-known that Cu^{2+} ions begin to electrodeposit without an accompanying overpotential from the aqueous solution. Therefore, this cathodic current corresponds to the deposition current of Cu. With increasing cathodic current, at around 10^{-5}A, the potential significantly polarizes to the less-noble region. This phenomenon seems to be caused by the diffusion control of Cu^{2+} ions. In the potential region less-noble than the equilibrium potential of Co, the cathodic current increases again at circa –0.8 V. It is also well-known that the electrodeposition of iron-group metals such as Ni, Co, and Fe is accompanied by the overpotential due to the rate determining multi-step reduction mechanism. Therefore, this increase in cathodic current is mainly caused by the deposition current of Co. It is well known that the potential dependence of growth rate for the nanowires corresponds well to the polarization curve for Cu and Co deposition.
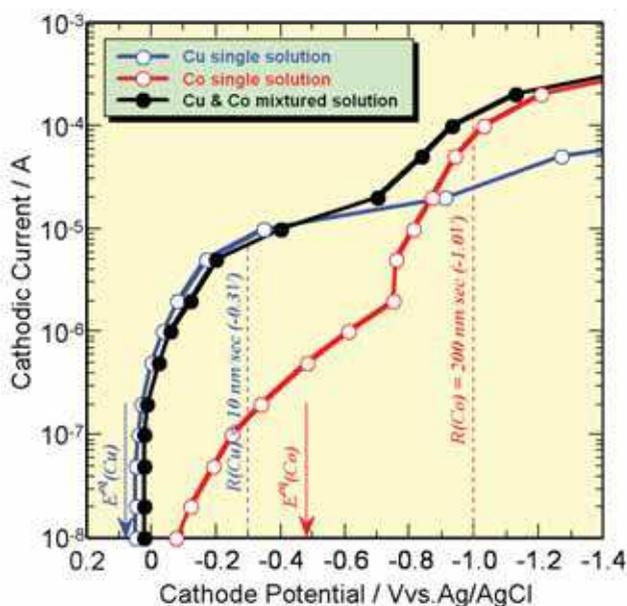

Fig. 16. Cathodic polarization curves for Cu (blue line), Co (red line) and Co-Cu alloy (black line) nanowires, both as a function of applied cathode potential during electrodeposition in a polycarbonate template with channel length 30 μm and diameter 200 nm.

Growth rates of nanowires were estimated by the channel filling time, which was determined from the time - dependence of deposition current at each potential.

Figure 17 shows the effect of the cathode potential on the time-dependence of the cathodic current during Co-Cu alloy nanowire deposition in the polycarbonate template with channel length 30 μm and diameter 200 nm. The cathode potentials were fixed to -0.7, -0.9, -1.1, and -1.3 V. To determine the wire growth rate, the channel-filling time was estimated by monitoring the deposition current. When the wires reach the membrane surface, the current will increase drastically due to the formation of hemispherical caps. If the radius of a hemispherical cap increases linearly with increase in deposition time, the current increases in proportion to the square of deposition time because the current linearly depends on the surface area of a hemispherical cap. Deposition rates were estimated by dividing channel length by channel-filling time. At –0.7 V, this time is around 600 s and the deposition rate is estimated to be about 50 nm s^{-1}, while the filling time is close to 60 s at –1.3 V and the deposition rate is estimated to be around 500 nm s^{-1}.
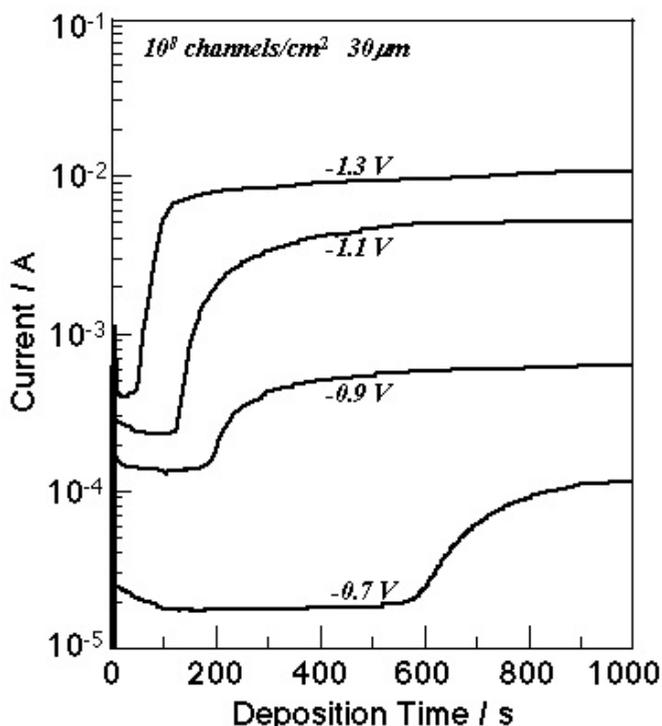

Fig. 17. Effect of cathode potential on measured current during Co-Cu alloy nanowire deposition in a polycarbonate template with channel length 30 μm and diameter 200 nm. The cathode potentials were -0.7, -0.9, -1.1, and -1.3 V.

On the basis of the results shown in Fig.16 and Fig.17, the optimum deposition potentials of Cu and Co are determined to be about –0.3 and –1.0 V (vs. Ag/ AgCl), that is, at potentials nobler than the diffusion limit region of each metal ion. Typical deposition rates of Cu and Co were roughly 10 nm s^{-1} (at –0.3 V) and 200 nm s^{-1} (at –1.0 V).

Co/ Cu multilayered nanowires were electrodeposited by alternatingly changing the cathode potential from -0.3 V vs. Ag/ AgCl (for Cu layer) to -1.0 V (for Co layer) as shown in Fig.18. According to this figure, when the potential is switched from -1.0 V to -0.3 V, anodic current is observed. This is resulting from the dissolution of electrodeposited Co, because -0.3V is more noble than the equilibrium potential of Co. At this potential, it is estimated that the Cu deposition and Co dissolution will proceed simultaneously.
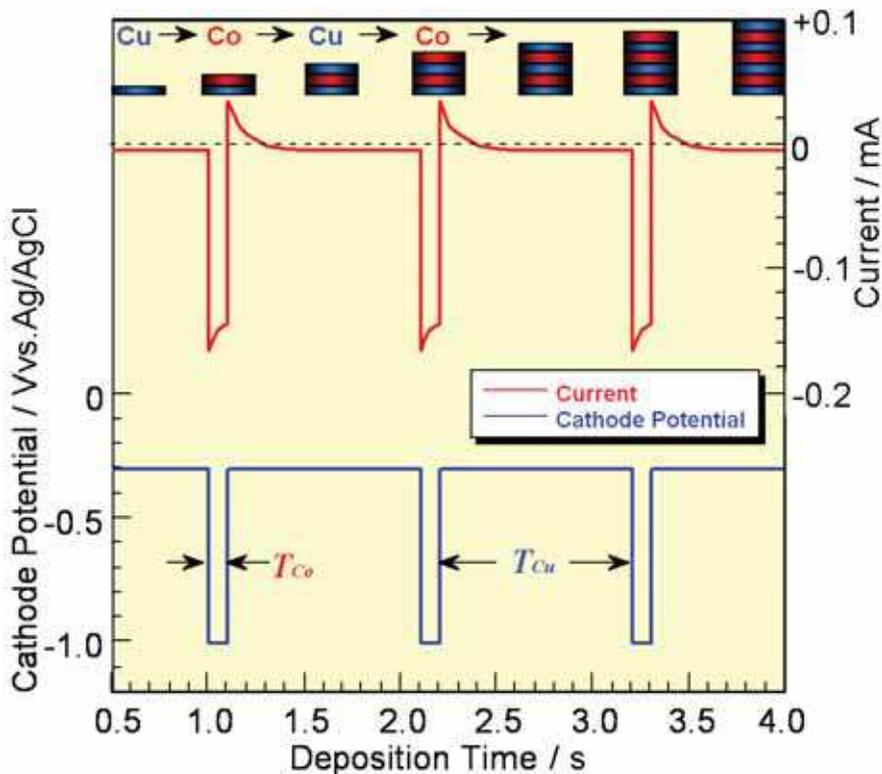

Fig. 18. Time dependence of observed-current and applied cathode potential during electrodeposition of Co/ Cu multilayered nanowires.

4.2 Crystal structure of Co/Cu multilayered nanowires

To determine the alloy composition of the wires, a sample was prepared as follows. First, nanowires were electrodeposited at constant cathode potential in polycarbonate channels with length 6 μm and diameter 40 nm. Then, the polycarbonate was dissolved in an organic solvent to expose the wires. Finally, the wire composition was determined by EDX. Co-Cu alloy nanowires electrodeposited at –1.0 V contained 81%-Co and 19%-Cu.

Figure 19 shows the SEM image and EDX profiles of electrodeposited Co/ Cu multilayered nanowires with the diameter of 40 nm and the each layer thickness of 30nm. According to the SEM image, multilayered structure is clearly observed and periodical EDX profiles also well correspond to the multilayered structure of the nanowires.
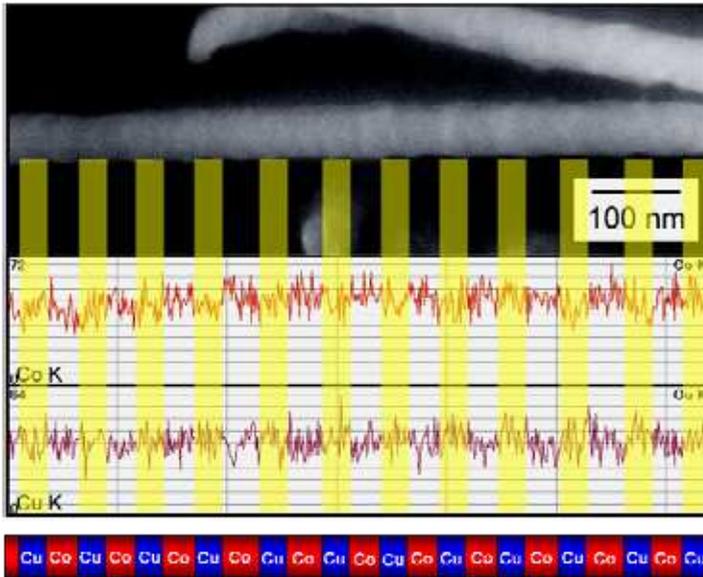
Fig. 19. SEM image and EDX profiles of electrodeposited Co/ Cu multilayered nanowires with the diameter of 40 nm and the each layer thickness of 30nm.

4.3 Magnetic properties of Co/Cu multilayered nanowires

To measure the wire resistance the wires were in-situ contacted with a gold layer during the electrodeposition process as illustrated in Fig.15-(d). Magneto-resistance curves were measured at room temperature applying a direct current of 10 μA and changing the magnetic field up to 10 kOe.

Figure 20 exhibits the magnetoresistive hysteresis of Co-Cu alloy nanowires and Co/ Cu multilayered nanowires electrodeposited in a polycarbonate template with channel length 30 μm and diameter 200 nm. Here, θ is defined as the angle between the magnetic field and the nanowire axis (current direction). The MR ratio is defined by the following equation

$$\text{MR ratio (\%)} = 100(R_0 - R_{10})/ R_{10} \qquad (7)$$

Here, R_0 and R_{10} are the resistance of zero field and 10 kOe, respectively. AMR curves of Co-Cu alloy nanowires show the usual dependence on the direction of the applied magnetic field. In the direction parallel to the wire (0 deg), the effect of magnetic field on the resistance was very small and the MR ratio was almost zero, while in the direction perpendicular to the wire (90 deg), the MR effect was maximum. An AMR ratio of 0.6 % was observed for $Co_{81}Cu_{19}$ alloy wires, which is typical of this system.

The structure of Co/ Cu nanowires electrodeposited in polymer templates is illustrated schematically in Fig.20. The layer thickness of Co and Cu is around to 10 nm. GMR strongly depends on Co and Cu layer thickness, and a maximum effect could be observed at about 10 nm. Therefore, a thickness of 10 nm was realized for each layer by controlling the deposition time. The GMR curves of Co/ Cu multilayered nanowires possess only a small angular dependence, and the MR ratio reaches up to 8.0 %. For these samples, the saturation field

seems to be around 5 kOe, which is much smaller than the field from which the AMR curves of Co-Cu alloy nanowires result. We have already reported that in porous alumina membranes Co/ Cu nanowires containing 100 and 300 bi-layers showed 20% and 12% of GMR ratio, respectively, while the Co/ Cu nanowires containing 1,500 bi-layers showed 8.0% in this study. It is not surprising that the GMR ratio of Co/ Cu nanowires will decrease when increasing the number of bi-layers. For example, this GMR decrease could be caused by the enhancement of Co/ Cu interfacial roughness with increasing the number of bi-layers.
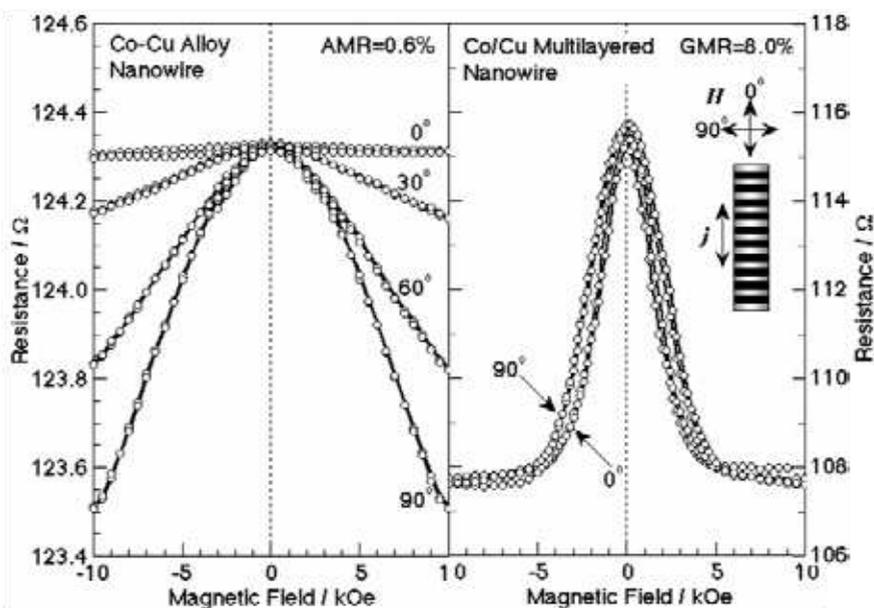

Fig. 20. Magnetoresistance of Co-Cu alloy nanowires and Co/ Cu multilayered nanowires with length 30 μm and diameter 200 nm electrodeposited in polycarbonate nanochannels. The layer thickness of Co and Cu is 10 nm.

Figure 21 shows the magnetoresistance of Co/ Cu multilayered nanowires with length 6 μm and diameter 60 nm electrodeposited in polycarbonate nanochannels. The each layer thickness of Co and Cu is adjusted to 10 nm. The GMR curves of Co/ Cu multilayered nanowires with length of 6 μm possess only a small angular dependence as well as the case of multilayered nanowires with length of 30 μm as shown in Fig.20. MR ratio of multilayered nanowires with length of 6 μm reaches up to 12 % as shown in Fig.21, which is much larger than that of multilayered nanowires with length of 30 μm. This is resulting from the difference of layered structure in nanowires. Layered structure will depend on the number of layers. With increasing number of layers, interlayer structure will be disappeared and each layer will form alloy. Therefore, GMR of multilayered nanowires with short length would show larger value than that of the multilayered nanowires with long length. Furthermore, GMR value will also depend on the magnetic domain structure in nanowires. It is well known that the magnetic domain structure depends on the diameter size of nanowires. With decreasing the diameter, the domain structure will be changed from multi-

domain to single domain. The domain wall in ferromagnetic layer will decrease GMR value. The domain wall area of nanowires with diameter 60 nm is smaller than that of nanowires with diameter 200 nm. Consequently, GMR of multilayered nanowires with short diameter would show larger value than that of the multilayered nanowires with long diameter.
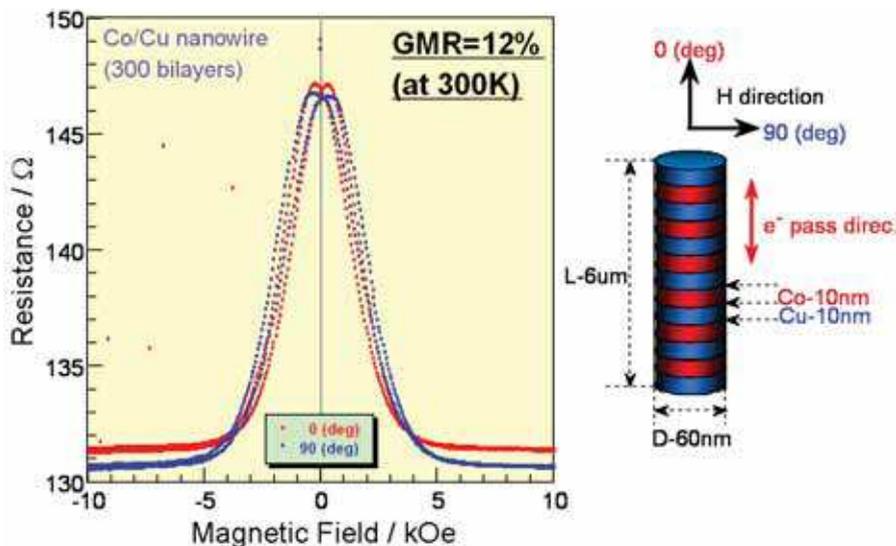

Fig. 21. Magnetoresistance of Co/ Cu multilayered nanowires with length 6 μm and diameter 60 nm electrodeposited in polycarbonate nanochannels. The layer thickness of Co and Cu is 10 nm. Magnetic field was applied to in-plan direction (blue line) and perpendicular direction (red line) to the membrane film plan. The perpendicular direction to the membrane film plan corresponds to the parallel direction to the long axis of nanowires.

5. Summary

5.1 Ni, Co and Fe nanowires
Optimum deposition potential region for growing Ni, Co and Fe nanowires was determined to be the range from –0.9 to –1.2 V. Growth rate of Ni nanowires was ca. 6 nm•sec⁻¹ at the cathode potential of –1.0 V. Growth rate of nanowires was increased up to around 30 nm•sec⁻¹ with increasing cathode potential up to -1.2 V.

The cylindrical shape was precisely transferred from the nanochannels to the nanowires and the aspect ratio reached up to ca. 150. The each nanowire was consisted of single crystalline domain. Basis on the uni-axial magnetic anisotropy and single magnetic domain structure of the ferromagnetic metal nanowires, the magnetic hysteresis loops showed typical perpendicular magnetization behavior and the coercive force reached up to around 1 kOe.

5.2 Ni-Fe alloy nanowires
Optimum deposition potential for electrodeposition of Ni-Fe alloy is determined to be ca. –1.0 V. Fe ratio in deposit was condensed more than 10 times higher than Fe^{2+} ratio in bath. This phenomena was explained by the anomalous codeposition mechanism due to the

formation and adhesion of $Fe(OH)_2$ on cathode. According to the mechanism, $Fe(OH)_2$ on cathode would suppress and inhibit the electrodeposition of Ni.

Coercive force of Ni-22at.Fe alloy film was ca. 1 Oe, which is quite smaller than that of Ni film (ca. 110 Oe). Ni-Fe alloy films with low coercive force were obtained over the wide range of Fe content from 20 % to 60 %.

Growth rate of Ni and Ni-Fe alloy nanowires was ca. 6 nm•sec^{-1} at the cathode potential of – 1.0 V. The cylindrical shape was precisely transferred from the nanochannels to the nanowires as well as the case of pure Ni and pure Fe nanowires.

Coercive force of Ni-22at.Fe alloy nanowires was ca. 100 Oe, which is almost half value of Ni nanowires (ca. 200 Oe). Magnetic hysteresis loops show unique soft magnetic behavior due to decreasing the uni-axial magnetic anisotropy resulting from the alloying effect of Fe.

5.3 Co/Cu multilayered nanowires

Optimum deposition potentials of Cu and Co are determined to be about –0.3 and –1.0 V (vs. Ag/ AgCl), that is, at potentials nobler than the diffusion limit region of each metal ion. Typical deposition rates of Cu and Co were roughly 10 nm s^{-1} (at –0.3 V) and 200 nm s^{-1} (at – 1.0 V). Co/ Cu multilayered nanowires were electrodeposited by alternatingly changing the cathode potential from -0.3 V vs. Ag/ AgCl (for Cu layer) to -1.0 V (for Co layer). Co-rich alloy electrodeposited at –1.0V consisted of 81%-Co and 19%-Cu.

GMR ratio of Co/ Cu multilayered nanowires with length 6 μm, diameter 60 nm and layer-thickness 10 nm reaches up to 12 %. GMR curves of the Co/ Cu multilayered nanowires showed only a small angular dependence. It was suggested that the interlayer structure will be disappeared and each layer will form alloy with increasing number of layers. Co/ Cu multilayered nanowires with short length and short diameter would show larger GMR value than that of the multilayered nanowires with long length and long diameter due to the magnetic domain structure.

6. References

Kawai, S. & Ueda, R. (1975). Magnetic properties of anodic oxide coatings on aluminum containing electrodeposited Co and Co-Ni. *J Electrochem. Soc*., Vol.122, Issue 1, (January 1975) 32-36, ISSN 0013-4651

Kawai, S. (1975). Retentivities of anodic oxide coatings on aluminum containing electrodeposited cobalt, nickel, and cobalt-nickel. *J Electrochem. Soc*., Vol.122, Issue 8, (August 1975) 1026-1029, ISSN 0013-4651

Kawai, S. & Ishiguro, I. (1976). Recording characteristics of anodic oxide films on aluminum containing electrodeposited ferromagnetic metals and alloys. *J Electrochem. Soc*., Vol.123, Issue 7, (July 1976) 1047-1051, ISSN 0013-4651

Tsuya, N.; Saito, Y.; Nakamura, H.; Hayano, S.; Furugohri, A.; Ohta, K.; Wakui, Y. & Tokushima, T. (1986). A perpendicular magnetic recording medium by alumite. *J Magn. Magn. Mater*., Vol.54-57, Part 3, (February 1986) 1681-1682, ISSN 0304-8853

Tsuya, N.; Tokushima, T.; Shiraki, M.; Wakui, Y.; Saito, Y.; Nakamura, H. & Katsumata, Y. (1987). Magnetic alumite disc for perpendicular recording. *IEEE Trans. Magn.* Vol.23, Issue 1, (January 1987) 53- 55, ISSN 0018-9464

Huysmans, G. T. A.; Lodder, J. C. & Wakui, J. (1988). Magnetization curling in perpendicular iron particle arrays (alumite media). *J Appl. Phys*., Vol.64, Issue 4, (August 1988) 2016-2021, ISSN 0021-8979

Ishiia, Y. & Sato, M. (1989). Magnetic behavior of a film with columnar structure. *J Magn. Magn. Mater.*, Vol.82, Issues 2-3, (December 1989) 309-312, ISSN 0304-8853

Cheng, T. -J.; Jorné, J & Gau, J -S. (1990). Magnetic anisotropy of electrodeposited cobalt on alumite substrate. *J Electrochem. Soc.*, Vol.137, Issue 1, (January 1990) 93-95, ISSN 0013-4651

Zhang, L. C. & Lodder, J. C. (1990). The influence of the packing density on the magnetic behaviour of alumite media. *J Magn. Magn. Mater.*, Vol.88, Issues 1-2, (July 1990) 236-246, ISSN 0304-8853

Martin, C. R. (1991). Template synthesis of polymeric and metal microtubules. *Adv. Mater.*, Vol.3, Issue 9, (September 1991) 457-459, ISSN 0935-9648

Aimawlawi, D.; Coombs, N. & Moskovits, M. (1991). Magnetic properties of Fe deposited into anodic aluminum oxide pores as a function of particle size. *J Appl. Phys.*, Vol.70, Issue 8, (October 1991) 4421-4425, ISSN 0021-8979

Whitney, T. M.; Jiang, J S.; Searson, P. C. & Chien, C. L. (1993). Fabrication and magnetic properties of arrays of metallic nanowires. *Science,* Vol.261, Issue 5126, (September 1993) 1316-1319, ISSN 0036-8075

Martin, C. R. (1994). Nanomaterials: a membrane-based synthetic approach. *Science,* Vol.266, Issue 5193, (December 1994) 1961-1966, ISSN 0036-8075

Piraux, L.; George, J M.; Despres, J. F.; Leroy, C.; Ferain, E.; Legras, R.; Ounadjela, K. & Fert, A. (1994). Giant magnetoresistance in magnetic multilayered nanowires. *Appl. Phys. Lett.*, Vol.65, Issue 19, (November 1994) 2484-2486, ISSN 0003-6951

Blondel, A.; Meier, J P.; Doudin, B. & Ansermet, J.-Ph. (1994). Giant magnetoresistance of nanowires of multilayers. *Appl. Phys. Lett.*, Vol 65, Issue 23, (December 1994) 3019-3021, ISSN 0003-6951

Dubois, S; Marchal, C.; Beuken, J. M.; Piraux, L.; Duvail, J L.; Fert, A.; George, J M. & Maurice, J L. (1997). Perpendicular giant magnetoresistance of NiFe/ Cu multilayered nanowires. *Appl. Phys. Lett.*, Vol.70, Issue 3, (January 1997) 396-398, ISSN 0003-6951

Hulteen, J C. & Martin, C. R. (1997). A general template-based method for the preparation of nanomaterials. *J Mater. Chem.*, Vol.7, Issue 7, (July 1997) 1075–1087, ISSN 0959-9428

Nielsch, K.; Müller, F.; Li, A. P. & Gösele, U. (2000). Uniform nickel deposition into ordered alumina pores by pulsed electrodeposition**.** *Adv. Mater.*, Vol.12, Issue 8, (April 2000) 582-586, ISSN 0935-9648

Evans, P. R.; Yi, G. & Schwarzacher, W. (2000). Current perpendicular to plane giant magnetoresistance of multilayered nanowires electrodeposited in anodic aluminum oxide membranes. *Appl. Phys. Lett.*, Vol.76, Issue 4 (January 2000) 481-483, ISSN 0003-6951

Forrer, P.; Schlottig, F.; Siegenthaler, H. & Textor, M. (2000). Electrochemical preparation and surface properties of gold nanowire arrays formed by the template technique. *J Appl. Electrochem.,* Vol.30, No.5, (May 2000) 533-541, ISSN 0021-891X

Sellmyer, D. J; Zheng, M. & Skomski, R. (2001). Magnetism of Fe, Co and Ni nanowires in self-assembled arrays. *J Phys.: Condens. Matter.,* Vol.13, Issue 25 (June 2001) R433-R460, ISSN 0953-8984

Sauer, G.; Brehm, G.; Schneider, S.; Nielsch, K.; Wehrspohn, R. B.; Choi, J; Hofmeister, H. & Gösele, U. (2002). Highly ordered monocrystalline silver nanowire arrays. *J Appl. Phys.*, Vol.91, Issue 5, (March 2002) 3243-3247, ISSN 0021-8979

Ohgai, T.; Hoffer, X.; Gravier, L.; Wegrowe, J. E. & Ansermet, J.-Ph. (2003). Bridging the gap between template synthesis and microelectronics: spin-valves and multilayers in self-organized anodized aluminum nanopores. *Nanotechnology,* Vol.14, Issue 9, (September 2003) 978-982, ISSN 0957-4484

Ohgai, T.; Hoffer, X.; Fabian, A.; Gravier, L. & Ansermet, J.-Ph. (2003). Electrochemical synthesis and magnetoresistance properties of Ni, Co and Co/Cu nanowires in nano-porous anodic oxide layer on metallic aluminum. *J. Mater. Chem.*, Vol.13, Issue 10, (October 2003) 2530-2534, ISSN 0959-9428

Enculescu, I.; Siwy, Z.; Dobrev, D.; Trautmann, C.; Toimil, Molares, M. E.; Neumann, R.; Hjort, K.; Westerberg, L. & Spohr, R. (2003). Copper nanowires electrodeposited in etched single-ion track templates. *Appl. Phys. A: Mater. Sci. Process.,* Vol.77, No.6, (November 2003) 751-755, ISSN 0947-8396

Ohgai, T.; Gravier, L.; Hoffer, X.; Lindeberg, M.; Hjort, K.; Spohr, R. & Ansermet, J.-Ph. (2003). Template synthesis and magnetoresistance property of Ni and Co single nanowires electrodeposited into nano-pores with wide range of aspect ratios. *J. Phys. D: Appl. Phys.,* Vol.36, Issue 24, (December 2003) 3109-3114, ISSN 0022-3727

Oh, J.; Tak, Y. & Lee, J. (2004). Electrodeposition of Cu_2O nanowires using nanoporous alumina template. *Electrochem. Solid-State Lett.*, Vol.7, Issue 3, (January 2004) C27-C30, ISSN 1099-0062

Wu, M. T.; Leu, I. C.; Yen, J. H. & Hon, M. H. (2004). Preparation of Ni nanodot and nanowire arrays using porous alumina on silicon as a template without a conductive interlayer. *Electrochem. Solid-State Lett.*, Vol.7, Issue 5, (March 2004) C61-C63, ISSN 1099-0062

Wang, W.; Huang, Q.; Jia, F. & Zhu, J. (2004). Electrochemically assembled p-type Bi_2Te_3 nanowire arrays. *J. Appl. Phys.,* Vol.96, Issue 1, (July 2004) 615-618, ISSN 0021-8979

Ohgai, T.; Hoffer, X.; Gravier, L. & Ansermet, J.-Ph. (2004). Electrochemical surface modification of aluminum sheets for application to nanoelectronic devices: anodization aluminum and electrodeposition of cobalt-copper. *J. Appl. Electrochem.,* Vol.34, No.10, (October 2004) 1007-1012, ISSN 0021-891X

Chu, S. Z.; Inoue, S.; Wada, K.; Kanke, Y. & Kurashima, K. (2005). Fabrication and characterization of integrated ultrahigh-density Fe-Pt alloy nanowire arrays on glass. *J. Electrochem. Soc.*, Vol.152, Issue 1, (December 2004) C42-C47, ISSN 0013-4651

Ohgai, T.; Gravier, L.; Hoffer, X. & Ansermet, J.-Ph. (2005). CdTe semiconductor nanowires and NiFe ferro-magnetic metal nanowires electrodeposited into cylindrical nano-pores on the surface of anodized aluminum. *J. Appl. Electrochem.,* Vol.35, No.5, (May 2005) 479-485, ISSN 0021-891X

Zhang, X.; Hao, Y.; Meng, G. & Zhang, L. (2005). Fabrication of highly ordered InSb nanowire arrays by electrodeposition in porous anodic alumina membranes. *J. Electrochem. Soc.*, Vol.152, Issue 10, (August 2005) C664-C668, ISSN 0013-4651

Fukunaka, Y.; Motoyama, M.; Konishi, Y. & Ishii, R. (2006). Producing shape-controlled metal nanowires and nanotubes by an electrochemical method. *Electrochem. Solid-State Lett.*, Vol.9, Issue 3, (January 2006) C62-C64, ISSN 1099-0062

Carlier, D. & Ansermet, J.-Ph. (2006). Electrochemical synthesis and magnetic properties of $CoFe_2O_4$ nanowire arrays. *J. Electrochem. Soc.*, Vol.153, Issue 5, (March 2006) C277-C281, ISSN 0013-4651

Ohgai, T.; Enculescu, I.; Zet, C.; Westerberg, L.; Hjort, K.; Spohr, R. & Neumann, R. (2006). Magneto-sensitive nickel nanowires fabricated by electrodeposition into multi- and single-ion track templates. *J Appl. Electrochem.,* Vol.36, No.10, (October 2006) 1157-1162, ISSN 0021-891X

Wang, X. W.; Fei, G. T.; Chen, L.; Xu, X. J & Zhang, L. D. (2007). Orientation-controllable growth of Ni nanowire arrays with different diameters. *Electrochem. Solid-State Lett.*, Vol.10, Issue 4, (February 2007) E1-E3, ISSN 1099-0062

Friedman, A. L. & Menon, L. (2007). Optimal parameters for synthesis of magnetic nanowires in porous alumina templates. *J Electrochem. Soc.*, Vol.154, Issue 4, (February 2007) E68-E70, ISSN 0013-4651

Katkar, R. A. & Tait, G. B. (2007). The effect of stationary ultraviolet excitation on the optical properties of electrochemically self-assembled semiconductor nanowires. *J Appl. Phys.*, Vol.101, Issue 5, (March 2007) 053508, ISSN 0021-8979

Inguanta, R.; Sunseri, C. & Piazza, S. (2007). Photoelectrochemical characterization of Cu_2O-nanowire arrays electrodeposited into anodic alumina membranes. *Electrochem. Solid-State Lett.*, Vol.10, Issue 12, (October 2007) K63-K66, ISSN 1099-0062

Riveros, G.; Gómez, H.; Schrebler, R.; Marotti, R. E. & Dalchiele, E. A. (2008). An in situ EIS study during the electrochemical growth of copper nanowires into porous polycarbonate membranes. *Electrochem. Solid-State Lett.*, Vol.11, Issue 3, (December 2007) K19-K23, ISSN 1099-0062

Kazeminezhad, I. & Schwarzacher, W. (2008). Electrodeposited Ni–Cu alloy nanowires with arbitrary composition. *Electrochem. Solid-State Lett.*, Vol.11, Issue 3, (January 2008) K24-K26, ISSN 1099-0062

Zhu, R.; Zhang, H.; Chen, Z.; Kryukov, S. & DeLong, L. (2008). Horizontally aligned single array of Co nanowires fabricated in one-dimensional nanopore array template. *Electrochem. Solid-State Lett.*, Vol.11, Issue 6, (April 2008) K57-K60, ISSN 1099-0062

Ohgai, T.; Hjort, K.; Spohr, R. & Neumann, R. (2008). Electrodeposition of cobalt based ferromagnetic metal nanowires in polycarbonate films with cylindrical nanochannels fabricated by heavy-ion-track etching. *J Appl. Electrochem.*, Vol.38, No.5, (May 2008) 713-719, ISSN 0021-891X

Ishizaki, T.; Saito, N. & Takai, O. (2009). Surfactant-assisted fabrication of tin oxide nanowires through one-step electrochemically induced chemical deposition. *J Electrochem. Soc.*, Vol.156, Issue 10, (August 2009) D413-D417, ISSN 0013-4651

Motoyama, M.; Dasgupta, N. P. & Prinz, F. B. (2009). Electrochemical deposition of metallic nanowires as a scanning probe tip. *J Electrochem. Soc.*, Vol.156, Issue 10, (August 2009) D431-D438, ISSN 0013-4651

Walton, A. S.; Górzny, M.; Bramble, J P. & Evans, S. D. (2009). Photoelectric properties of electrodeposited copper (I) oxide nanowires. *J Electrochem. Soc.*, Vol.156, Issue 11, (September 2009) K191-K195, ISSN 0013-4651
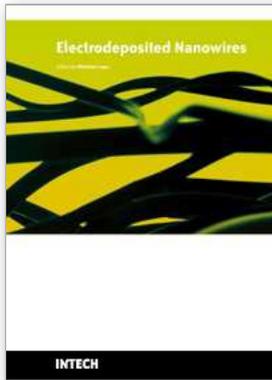
Electrodeposited Nanowires and their Applications

Edited by Nicoleta Lupu

The book offers a new and complex perspective on the fabrication and use of electrodeposited nanowires for the design of efficient and competitive applications. While not pretending to be comprehensive, the book is addressing not only to researchers specialized in this field, but also to Ph.D. students, postdocs and experienced technical professionals.

How to reference

In order to correctly reference this scholarly work, feel free to copy and paste the following:

Takeshi Ohgai (2010). Fabrication of Functional Metallic Nanowires Using Electrodeposition Technique, Electrodeposited Nanowires and their Applications, Nicoleta Lupu (Ed.), ISBN: 978-953-7619-88-6, InTech, Available from: http://www.intechopen.com/books/electrodeposited-nanowires-and-their-applications/fabrication-of-functional-metallic-nanowires-using-electrodeposition-technique

INTECH

open science | open minds